Journal of Solid Mechanics Vol. 15, No. 4 (2023) pp. 383-401
DOI: 10.60664/jsm.2024.3031772

Research Paper

Simulation of residual stress and distortion in welded carbon steel pipe by considering solid-state phase transformation

M.R. Jahanban, S. Feli *

Department of Mechanical Engineering, Razi University P.O. Box: 6714414971, Kermanshah, Iran

Received 3 March 2023; accepted 3 July 2023

ABSTRACT

In this paper, a sequentially coupled 3-D thermal-metallurgical-mechanical analysis is developed to predict welding residual stresses and distortion during single-pass tungsten inert gas arc welding (TIG) of low and medium carbon steel pipes (S45C and S15C). The axial and hoop residual stresses and welding deformation by allowing volumetric change due to solid-state phase transformation are determined. In ABAQUS finite element simulation, the moving heat source is modeled by a user subroutine [DFLUX], and a user subroutine [UEXPAN] is applied for computing the fraction of martensite and volume change during heating and cooling. The simulation results show that for the S15C pipe, solid-state phase transformation has an insignificant effect on welding residual stress and distortion but for the S45C pipe the solid-state phase transformation reduces the axial residual stress in the fusion (FZ) and heat-affected zones (HAZ). Also, the sign of hoop residual stress changes in FZ, and its value of it decreases in HAZ.

Keywords: Welded carbon steel pipe; Solid-State phase transformation; Welding residual stress; Distortion; ABAQUS.

1 INTRODUCTION

WELDING is a popular manufacturing procedure that is used extensively in steel structures. A weldment is heated locally by the welding heat source and the temperature in the vicinity of the weldment is not uniform and changes with distance from the weld centerline. Due to localized heating, complex thermal stresses are generated during welding.

Residual stresses remain in a metal material as a result of liquid-to-solid phase transformation associated with weld solidification and non-uniform cooling of the weld. High residual stresses in regions near the weld may promote brittle fractures, fatigue, or stress corrosion cracking. Also, residual stresses in the base metal may reduce the buckling strength of the structure members.

* Corresponding author. Tel.: +98 (83) 34274535-9, Fax: +98 (83) 34274542.
E-mail address: felisaeid@razi.ac.ir (S. Feli)

In carbon steels, for determining the residual stress and distortion accurately, metallurgical phase transformation must be considered. In the past decades, several numerical models have been proposed to predict residual stress in welded structures that consider the effects of solid-state phase transformation.

Deng and Murakawa [1] investigated the effects of volumetric change in welding residual stress by numerical analysis in butt-welded modified 9Cr-1Mo steel pipes. They showed that if the volumetric change due to phase transformation is considered, the simulation results are generally in good agreement with the experimental measurements.

Yaghi et al. [2] simulated welding and residual stresses in a P91 steel pipe incorporating solid-state phase transformation. The simulation results indicated that in the weld metal, solid-state phase transformation has a significant effect on residual stresses.

Deng and Murakawa [3] considered the effects of austenite-bainite and austenite-martensite transformations in multi-pass butt-welded 2.25Cr-1Mo steel pipes. They developed a thermal-metallurgical-mechanical computational procedure to simulate the welding temperature field, microstructure, and residual stress. The simulation results indicated that both volumetric change and yield strength change due to solid-state phase transformation have significant effects on welding residual stress.

Deng [4] investigated the effects of volume change due to austenite-martensite transformation on the final residual stress and the welding distortion in low and medium-carbon steel plate welds. The simulation results showed that for medium carbon steel, phase transformation has a significant effect on the welding residual stress and distortion.

Chin-Hyung Lee and Kyong-Ho Chang [5] predicted welding residual stresses in circumferentially butt-welded high-strength carbon steel pipes. A sequentially coupled 3-D thermal, metallurgical, and mechanical FE model by considering solid-state phase transformation during welding thermal cycles was employed. The results indicated that solid-state phase transformation has a very small effect on the axial residual stresses.

Feli et al [6], investigated the effects of heat flux distribution, latent heat, and heat flux type on the temperature field and residual stresses of butt-welded stainless steel pipes by ABAQUS. In this simulation, solid-state phase transformation had not considered. For verification of FE modeling the temperature fields and residual stresses were compared with available experimental results. The results showed that heat flux with a double ellipsoidal distribution proposed by Goldak was associated with latent heat parameters and employed a fully volumetric arc heat input, representing the best match with the experimental data.

Sendong Ren et al [7], used a full-scale finite element model for determining the stress distribution on 2.25Cr-Mo welded pipe. A moving heat source was employed to describe the welding heat input. Diffusive and displacive phase transformations were considered in the material model. In this simulation, the tempering effect and creep were considered crucial phenomena during welding. The simulation results showed that solid-state phase transformation could induce an undulating stress profile and large stress gradient in the welded zone.

Obeid Obeid et al [8], investigated the influence of girth welding material on thermal and residual stress fields in welded lined pipes. A pre-heat treatment was required to produce lined pipe specimens taken into account. The results indicated that replacing the girth welding mild steel with austenitic stainless steel has a significant effect on the residual stresses but no influence on the thermal history.

Parviz Asadi et al [9], studied the effects of material type and preheating and weld pass number on residual stress of welded steel pipes by multi-pass TIG welding. Results showed that the base material type has a greater effect on the tensile axial residual stress of the outer surface rather than that of the inner surface. However, the welding pass number showed no significant influence on the peak of the tensile axial residual stress on the inner surface of the pipe.

The influence of heat treatment in multi-pass dissimilar welded rotor joints of steel alloy was studied by Rajiv Kumar et al [10]. The effect of the post-weld on the distribution of residual stress was also investigated using both experimental and numerical approaches. The obtained findings revealed that apart from the weld centerline, hoop tensile residual stresses were higher around the buttered layer of Alloy 617 and 10Cr steel in an as-welded state. Also, 80% of the stresses generated along the weld section have been released after the post-weld.

In this paper, a new simulation procedure has been used for determining the residual stresses and distortion during single-pass Tungsten inert gas arc welding in low and medium-carbon steel of butt-welded pipes. The influence of solid-state phase transformation by allowing for volumetric change due to solid-state phase transformation has been considered and the axial and hoop residual stresses and welding deformation have been determined. Considering the effects of solid-state phase transformation by allowing volumetric change, moving heat source by a user subroutine [DFLUX] in ABAQUS code, using the [UEXPAN] subroutine for computing the fraction of martensite and volume change during heating and cooling, are the innovations discussed.

2 FE SIMULATION OF THE WELDING PROCESS

Numerical simulation of the thermal–mechanical process associated with residual stress evolution during welding can be extremely complex since it needs to take into account the interactions between heat transfer, metallurgical transformation, and mechanical fields. Complex numerical approaches are then needed to accurately model the welding process.

In this paper, thermal and mechanical analyses are carried out sequentially. The solution procedure consists of two steps. In the first step, the thermal analysis solves for the transient temperature history associated with the heat flow during welding. The thermal analysis is based on the heat conduction formulation with the moving heat source. In the next step, the resulting temperature history is applied as a thermal load for the stress evolution in the subsequent mechanical analysis and the volume fraction of martensite is also determined. The volume change due to phase transformation is considered by modifying the thermal expansion coefficient over the temperature range in which austenite changes into martensite. Therefore a subroutine to the ABAQUS code [UEXPAN] is developed to compute the fraction of martensite and volume change during heating and cooling.

2.1 Model geometry and material properties

The 3-D finite element model is shown in Fig. 1 with 11648 brick elements and 15120 nodes. The welding arc travel direction and welding start/stop position (θ=0°) are illustrated. Because of the symmetry, one-half of the model is selected as the analysis model. It has a fine grid in the welding zone. The smallest element size is 1*1.5*3.2 (mm). The length, outer diameter, and thickness of the model are 400 mm, 114.3 mm, and 6 mm, respectively.

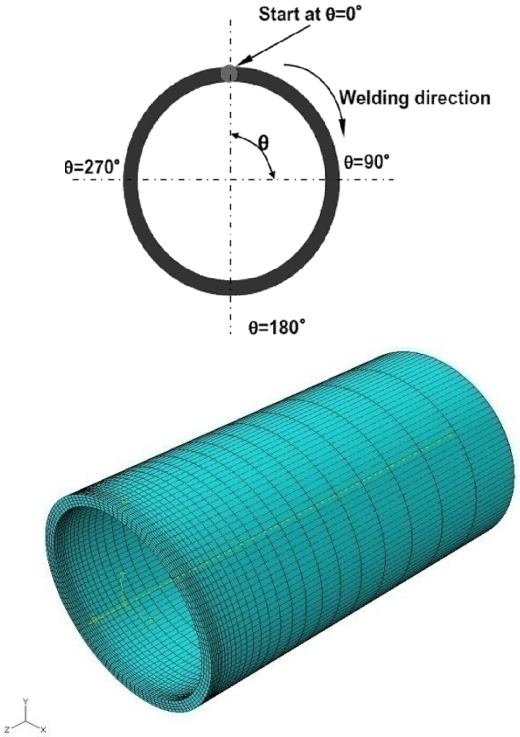

Fig.1
3-D finite element model and welding direction.

To clarify the effect of phase transformation on welding residual stress and deformation, two types of steel, including low carbon steel (S15C) and medium carbon steel (S45C), are selected. The chemical compositions, thermal and mechanical properties versus temperature are shown in Table 1, and Fig. 3 [4], respectively. This study assumed that the thermal properties of S15C steel are the same as those of S45C steel.

Table 1.
Chemical composition of S15C and S45C Steel,wt%[4]

Steel	C	Mn	Si	Cr	S	P
S45C	0.44	0.66	0.22	0.15	0.029	0.022
S15C	0.15	0.41	0.22	0.06	0.024	0.021

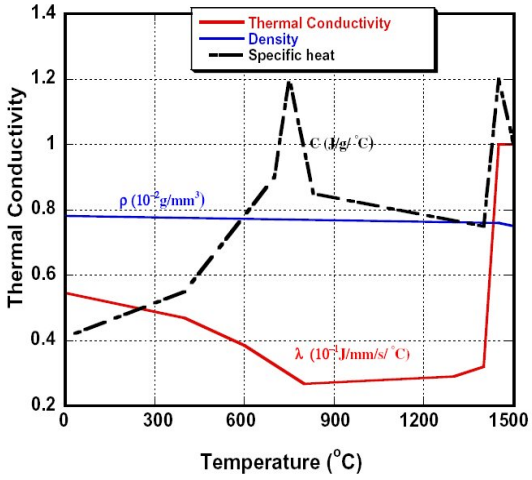

Fig.2
Temperature-dependent thermal-physical properties [4].

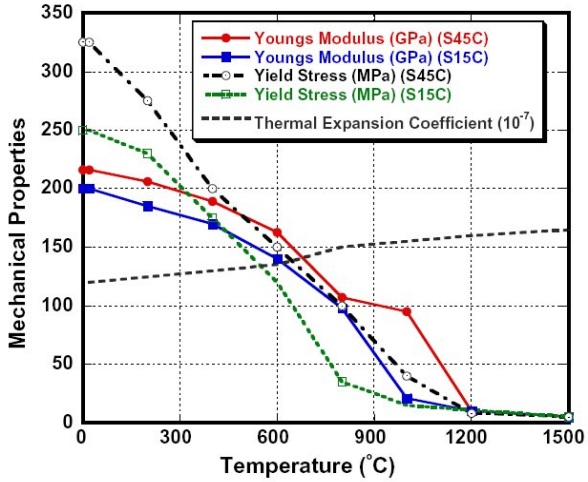

Fig.3
Temperature-dependent mechanical-physical properties [4].

2.2 Thermal Analysis

In this study, the heat from the moving welding arc is applied as a volumetric heat source with a double ellipsoidal distribution proposed by Goldak et al. [11], which is expressed by the following equations:

For the front heat source:

$$q_f(x,y,z,t) = \frac{6\sqrt{3} f_f Q}{abc_f \pi \sqrt{\pi}} e^{-3x^2/a^2} e^{-3y^2/b^2} e^{-3z^2/c_f{}^2} \tag{1}$$

For the rear heat source:

$$q_r(x,y,z,t) = \frac{6\sqrt{3} f_r Q}{abc_r \pi \sqrt{\pi}} e^{-3x^2/a^2} e^{-3y^2/b^2} e^{-3z^2/c_r{}^2} \tag{2}$$

Where x_0, y_0, and z_0 are the local coordinates of the double ellipsoid model aligned with the welded pipe; f_f and f_r are parameters that give the fraction of the heat deposited in the front and the rear parts, respectively. Note that $f_f + f_r = 2.0$. The temperature gradient in the front leading part is steeper than in the tailing edge [12] therefore the ff and fr are assumed to be 1.4 and 0.6, respectively. The Qw is the power of the welding heat source and can be calculated according to the welding current, arc voltage, and arc efficiency. The arc efficiency γ is assumed to be 70% for the TIG welding process. The parameters a_1, a_2, b, and c are related to the characteristics of the welding heat source. The parameters of the heat source can be adjusted to create a desired melted zone according to the welding conditions. The moving heat source is modeled by a user subroutine in ABAQUS code [DFLUX]. The liquid-to-solid phase transformation effects of the weld pool are modeled by taking into account the latent heat of fusion. The latent heat is assumed value of 270 J/g between the solidus temperature of 1430 °C and the liquid temperature of 1480°C [19]. The welding conditions are given in Table 2.

Table 2
Welding conditions[4]

Current(A)	Voltage(V)	Speed(mm/s)
300	21	10

Both the thermal radiation and heat transfer on the weld surface are considered. Radiation losses are dominating for higher temperatures near the weld zone, and convection losses for lower temperatures away from the weld zone. A user subroutine [FILM] is developed to simulate the combined thermal boundary conditions. The total temperature-dependent heat transfer coefficient is given by Eq. (3) [14].

$$h = \begin{cases} 0.0668T & W/m^2 \qquad 0 < T < 500^\circ C \\ 0.231T - 82.1 & W/m^2 \qquad T > 500^\circ C \end{cases} \tag{3}$$

Where T is the temperature.

2.3 Solid-state phase transformation

2.3.1 Phase transformation during heating

Solid state phase transformation is responsible for changes in both volume and yield stress in steel experiencing thermal cycles during welding. In carbon steel, martensitic transformation, which occurs during rapid cooling immediately after intense welding heat input, is the phase transformation associated with significant volumetric and yield stress change.

The metallurgical structure of the steel is assumed to be pearlite–ferrite before any thermal cycles take place. During welding, when the steel reaches the temperature A1 (cementite disappearance temperature), it begins to transform from pearlite–ferrite to austenite, and when the temperature reaches A3 (a-ferrite disappearance temperature), the austenite transformation is assumed to be complete and the material fully austenitic. Pearlite–ferrite steel has a b.c.c. structure, whereas austenite has a f.c.c. structure. During austenite transformation the steel undergoes a reduction in volume, as can be schematically shown in Fig. 4. Also the phase transformation temperatures of S15C and S45C steel are given in Table 3.

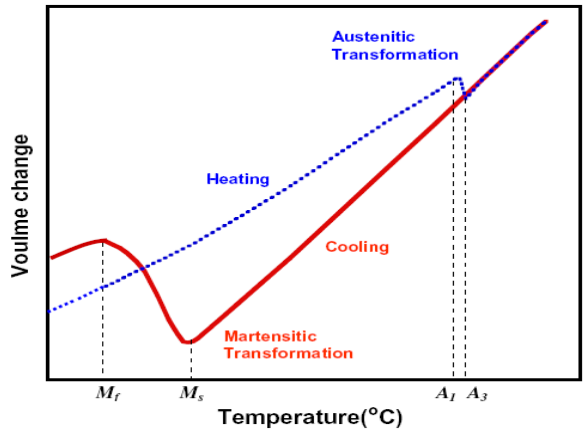

Fig.4
Schematic diagram of volume change due to phase transformation.

Table 3

Phase transformation temperatures of S15C steel and S45C Steel [4]

Steel	A_1	A_3	M_S	Mf
S45C	724	787	328	140
S15C	726	843	476	280

A linear relation is assumed to simulate the formation of austenite. This relation can be written as follows:

$$f_a = \frac{T - A_1}{A_3 - A_1} \qquad (A_1 \leq T \leq A_3) \tag{4}$$

By using the linear approximation, the increment of the austenite volume fraction (Δf_a) at each step is estimated by:

$$\Delta f_a = \frac{\Delta T}{A_3 - A_1} \qquad (A_1 \leq T \leq A_3) \tag{5}$$

Where ΔT is the increment temperature at the current step during heating.

Also for both S45C and S15C steel, the volume change due to austenite transformation is assumed to be $\varepsilon_{\Delta vol}^{A*} = -2.88 \times 10^{-3}$ (6).[15]

By using relations (5) and (6), the strain increment can be estimated as follows:

$$\Delta\varepsilon_{\Delta vol}^{A} = \Delta f_a . \varepsilon_{\Delta vol}^{A*} \tag{6}$$

$$\Delta\varepsilon_{\Delta vol}^{A} = -\frac{2.88\times10^{-3}\Delta T}{A_3 - A_1} \tag{7}$$

Investigation above relation shows that in the temperature range $(A_1 \leq T \leq A_3)$ the sign of volumetric change strain increment is negative.

2.3.2 Martensite transformation

After the heating phase and formation of austenite, continue cooling causes that fcc mesh of austenite to transform into bcc mesh of ferrite and cementite phase by the following relation:

$\gamma \rightarrow \alpha + Fe3C$ (8)

To form of ferrite, extra atoms of carbon must penetrate from the octahedral spaces of bcc into the cementite phase. If the cooling process is sufficiently rapid, atoms of carbon in octahedral spaces of bcc mesh are convicted and they can't penetrate. Therefore atoms of carbon increase the height of the mesh and thus austenite transforms into martensite with a b.c.t. structure, and the volume increases, which can also be seen in Fig. 4.

In the simulation, an integration point of an element for transform to martensite phase has two conditions. At first for the transform to austenite phase, the maximum temperature in the heating process should be greater than A3. With increasing temperature, grains will be large and grains boundary will be small. The hardness and percent of obtained martensite phase will increase. Therefore in simulation, the CCT diagram is used for the region of HAZ which is located near the fusion zone and has a high temperature (1050°C-1450°C) that is called the coarse-grained heat-affected zone and is different from the region of HAZ which is located far away weld line and have a lower temperature (A3-1050°C) that is calling fine-grained heat affected zone The second condition is the cooling time from 800°C to 500°C that should be less than the critical cooling time. All of the alloy elements except cobalt with a solution in austenite causes the CCT diagram to move to the right. This effect of alloy elements reduces the critical cooling gradient and convenient to get the martensite phase. Therefore all of the high alloy steels with cooling in the air will be full martensite and simple carbon steels to transform to martensite phase completely, must cool in water or oil. But in welding simple carbon steels similar to present work which quench environment is air, they can't transform to martensite completely. In these steels, the obtained martensite phase is sensitive to cooling time. Therefore in simulation by using temperature history peak temperature and cooling time from 800°C to 500°C for each node must be determined.

An infinite number of CCT diagrams must explain transformation behavior in every region of the weld metal and the HAZ. In this paper, the relationship between the cooling rate and the fraction of martensite is obtained from CCT diagrams with austenitization temperatures 900 °C and 1050 °C to predict the fraction of martensite for the fine-grained HAZ and the coarse-grained HAZ, respectively. These diagrams for both kinds of material are presented by Deng [4].

On cooling the martensite transformation can be described using the Koistinen–Marburger relationship [16]:

$$f_m(T) = f\left[1 - \exp\left(-b(Ms - T)\right)\right] \qquad (T \leq M_s) \tag{9}$$

where T is the current temperature during cooling; f represents the obtained martensite phase whose magnitude of that is almost one for high alloy steels and for simple carbon steel is a function of cooling rate and maximum temperature; MS is the martensite start temperature and the constant b represents the evolution of martensite transformation process according to temperature. For carbon steel and low alloy steel, the value of b is 0.011; fm is the volume fraction of obtained martensite phase at the current temperature (°C).

Generally, the retained austenite cannot fully change into martensite during welding, and the remained percentage mainly depends on the chemical components and the temperature history, so a modified Koistinen–Marburger relationship is used in the present simulations. The modified equation is explained as follows [3]:

$$f_m(T) = f_{mod}.f\left[1 - \exp\left(-b(Ms - T)\right)\right] \qquad (M_f \leq T \leq M_s) \tag{10}$$

Where f_{mod} is the modified coefficient. This modified coefficient is defined as follows:

$$\begin{aligned} &T = Ms \rightarrow f_m = 0 \\ &T = Mf \rightarrow f_m = 1 \rightarrow f_{mod} = 1/\left[1 - \exp\left(-b(Ms - Mf)\right)\right] \end{aligned} \tag{11}$$

In the finite element models, the differential equation derived from Eq. (10) was used to calculate the increment of the martensite volume fraction. For example, the increment of martensite volume fraction can be expressed as follows:

$$\Delta f_m = f_{mod}.f\left\{-0.011\exp[0.011(T - Ms)]\right\} \cdot \Delta T \qquad (M_f \leq T \leq M_s) \tag{12}$$

Where ΔT is the temperature increment during cooling.

Also, the strain due to volume change associated with full martensitic transformation assigned to S45C steel and S15C steel is $\varepsilon_{\Delta vol}^{M*} = 8.0 \times 10^{-3}$ and $\varepsilon_{\Delta vol}^{M*} = 2.0 \times 10^{-3}$ [17], respectively. Therefore the strain increment can be estimated as follows:

$$\begin{aligned} &\Delta\varepsilon_{\Delta vol}^{M} = \Delta f_m.\varepsilon_{\Delta vol}^{M*} \\ &\Delta\varepsilon_{\Delta vol}^{M} = f_{mod}.f\left\{-0.011\exp[0.011(T - Ms)]\right\}.\Delta T.\varepsilon_{\Delta vol}^{M*} \end{aligned} \tag{13}$$

2.4 Mechanical analysis

The same finite element model used in the thermal analysis was employed here, except for the element type and the boundary conditions. The solid element type used in the mechanical analysis is an 8-node bi-quadratic stress/displacement quadrilateral with reduced integration (C3D8R). Because of the symmetry of the FE model and reduce of computational time half of the model is selected as the analysis model. Therefore a symmetry condition for the weld surface relative to the axis of the pipe (z-axis) is considered. Also to prevent rigid body motion of weld pipe, two points at the top and the bottom end of pipe are constrained in x and y directions. The mechanical analysis is conducted using the temperature histories computed by the thermal analysis.

During the welding process, along with the thermal strain, an additional strain is induced by the microstructure evolution during solid-state phase transformation. The phase transformation also produces transformation-induced plasticity. This can be represented analytically by adding a separate strain component to the total strain function.

Hence, the total strain rate $(\dot{\varepsilon})$ for a steel undergoing solid-state phase transformation can be written as the sum of the individual components of the strain rate as follows:

$$\dot{\varepsilon} = \dot{\varepsilon}_E + \dot{\varepsilon}_p + \dot{\varepsilon}_T + \dot{\varepsilon}_{\Delta Vol} + \dot{\varepsilon}_{Trp} \tag{14}$$

$\dot{\varepsilon}_E$, $\dot{\varepsilon}_p$, $\dot{\varepsilon}_T$, $\dot{\varepsilon}_{\Delta Vol}$, $\dot{\varepsilon}_{Trp}$ are the strain rate components due to elastic, plastic and thermal loading, volumetric change and transformation plasticity, respectively. In this study, transformation induced plasticity is not taken into account. Ignoring this component the strain increments can be expressed by the following equation:

$$\Delta\varepsilon_{total} = \Delta\varepsilon_E + \Delta\varepsilon_p + \Delta\varepsilon_T + \Delta\varepsilon_{\Delta Vol} \tag{15}$$

The elastic strain increment $\Delta\boldsymbol{\varepsilon}_{\mathbf{E}}$ is calculated using the isotropic Hook's law with temperature-dependent Young's modulus and Poisson's ratio. The thermal strain increment $\Delta\boldsymbol{\varepsilon}_{\mathbf{T}}$ is computed using the coefficient of thermal expansion. For the plastic strain increment $\Delta\boldsymbol{\varepsilon}_{\mathbf{p}}$, a rate-independent plastic model is employed with the following features: the Von Mises yield surface, temperature-dependent mechanical properties, and linear kinematic hardening model. The volumetric change strain increment $\Delta\boldsymbol{\varepsilon}_{\Delta\mathbf{vol}}$ is calculated using Eqs. (7) and (13), and then added to the thermal strain component $\Delta\boldsymbol{\varepsilon}_{\mathbf{T}}$ in order to obtain the overall effect of volumetric change on the thermal expansion coefficient [2]. Hence, for martensitic transformation, strain due to both thermal loading and volumetric change can be expressed as:

$$\begin{aligned}\Delta\varepsilon_T + \Delta\varepsilon^{M}_{\Delta vol} &= (\alpha.\Delta T) + \Delta f_m.\varepsilon^{M*}_{\Delta vol} \\ &= (\alpha + f_{mod}.f\{-0.011\exp[0.011(T - Ms)]\}.\varepsilon^{M*}_{\Delta vol}).\Delta T\end{aligned} \tag{16}$$

Where the coefficient of thermal expansion is given in Fig. 3:

For austenitic transformation, strain due to both thermal loading and volumetric change is given by:

$$\begin{aligned}\Delta\varepsilon_T + \Delta\varepsilon^{A}_{\Delta vol} &= (\alpha.\Delta T) + \Delta f_a.\varepsilon^{A*}_{\Delta vol} \\ &= \left(\alpha + \frac{\varepsilon^{A*}_{\Delta vol}}{A_3 - A_1}\right).\Delta T\end{aligned} \tag{17}$$

The resultant function is the original coefficient of thermal expansion over the corresponding phase transformation temperature ranges.

3 RESULTS AND DISCUSSIONS

To validate the simulation procedure, the authors of this article [6], the temperature history and axial and hoop residual stresses in the inside and outside surfaces of the pipe which were computed by ABAQUS simulations compared with the experimental results of reference [18], It was observed that the values of the temperature history, axial and hoop residual stresses in inside and outside surfaces of pipe had an acceptable agreement with experimental results. In those comparisons, the influence of solid-state phase transformation was not considered.

In this paper, two different cases, Case 1 and Case 2, are simulated to clarify the effect of solid-state phase transformation on welding residual stresses and distortions. Case 1 does not incorporate solid-state phase transformation in the FE simulation. On the contrary, Case 2 takes solid-state phase transformation into account by allowing for volumetric changes due to solid-state phase transformation. Also To clarify the effect of carbon percentage on phase transformation, two kinds of steel, namely low carbon steel (S15C) and medium carbon steel (S45C), are selected.

3.1 Analysis of residual stress

In this section, the effect of the phase transformation of austenite to martensite at the path of θ=140° on the inner and outer surfaces of the pipe is investigated.

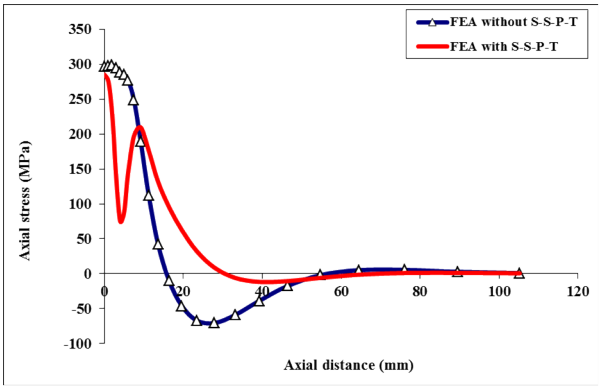

Fig.5
Predicted axial residual stress distribution on the inner surface with and without solid-state phase transformation of S45C pipe.

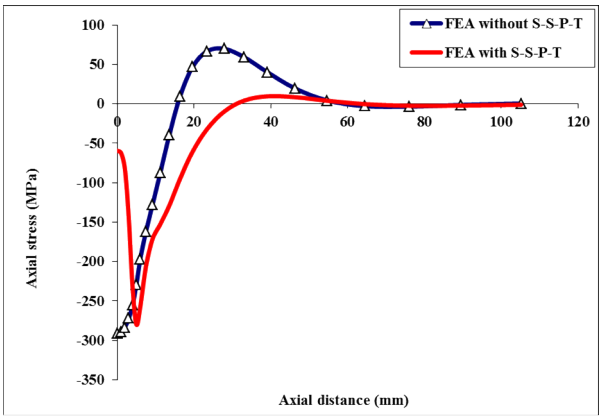

Fig.6
Predicted axial residual stresses distribution on the outer surface with and without solid-state phase transformation of S45C pipe.

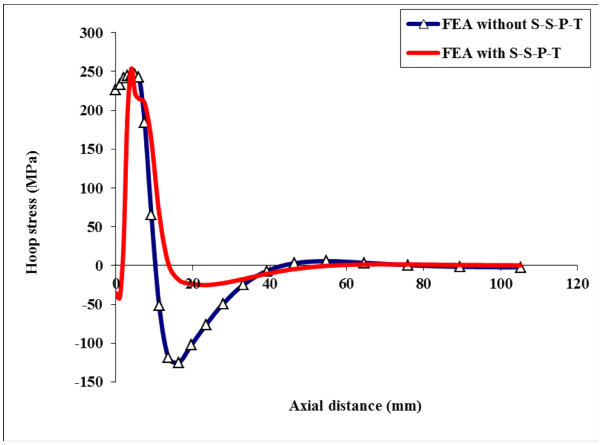

Fig.7
Predicted hoop residual stresses distribution on the inner surface with and without solid-state phase transformation of S45C pipe**.**

Fig. 5 and 6 show the axial residual stress distribution on the inner and outer surfaces of the S45C pipe with and without considering the effect of phase transformation. It can be found that phase transformation reduces the tensile residual stresses and compressive residual stresses in FZ and HAZ, respectively.

Fig. 7 and 8 show the hoop residual stress distribution on the inner and outer surfaces of the S45C pipe with and without considering the effect of phase transformation. These figures show that phase transformation causes tensile residual stress to change to compressive residual stress in the fusion zone and the value of hoop residual stress has decreased in HAZ. From relation (13), in the temperature range $(M_f \leq T \leq M_s)$ the sign of volumetric change strain increment is positive. This means that the material during the cooling process after the pass of welding heat source instead of shrinkage has expanded. This matter is caused by the formation of residual stresses that alter and tensile residual stresses have changed to compressive residual stresses.

Fig. 9 to 12 show the axial and the hoop residual stresses distribution on the inner and outer surfaces of the S15C pipe with and without considering the effect of solid-state phase transformation. It can be seen that phase transformation has high little effect on the residual stresses. Because a low percentage of carbon causes, volume dilation due to phase transformation is relatively small and the transformation temperature is relatively high [19].

3.2. Analysis of welding deformation

3.2.1. Deformations on a vertical cross-section area in HAZ

At first, a circular path (path 1 in fig. 13) in the middle of the thickness of a cross-section area at location (Z=3mm) in HAZ, verticals to the axis of the pipe is defined and displacements of nodes on the path 1 in the radial, hoop and axial directions are investigated.

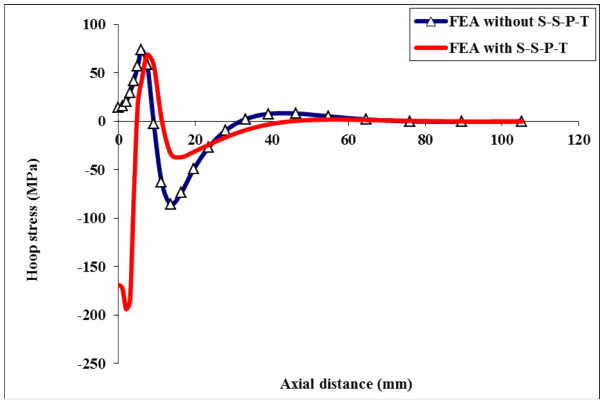

Fig.8
Predicted hoop residual stresses distribution on the outer surface with and without solid-state phase transformation of S45C pipe.

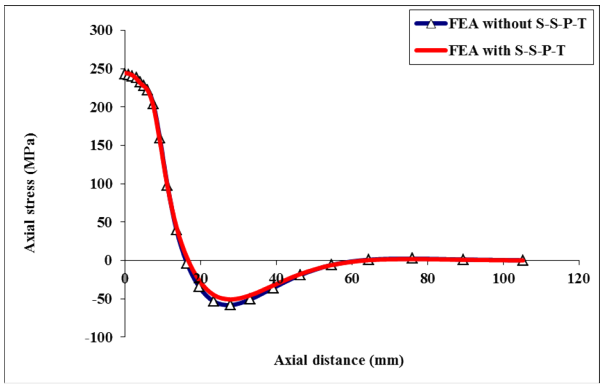

Fig.9
Predicted axial residual stresses distribution on the inner surface with and without solid-state phase transformation of

S15C pipe.

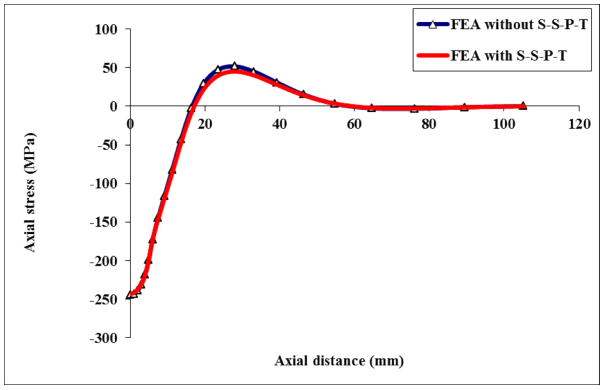

Fig.10
Predicted axial residual stresses distribution on the outer surface with and without solid-state phase transformation of S15C pipe**.**

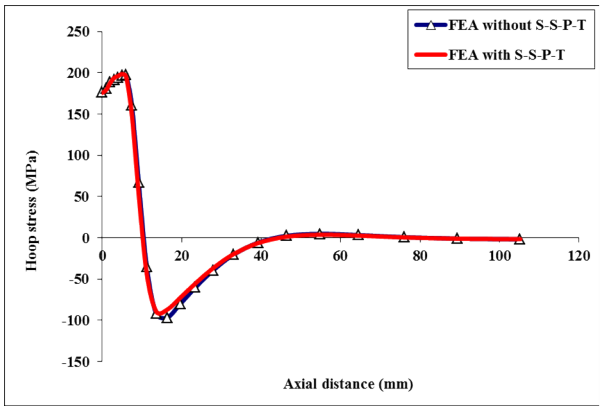

Fig.11
Predicted hoop residual Stresses distribution on the inner surface with and without solid-state phase transformation of S15C pipe**.**

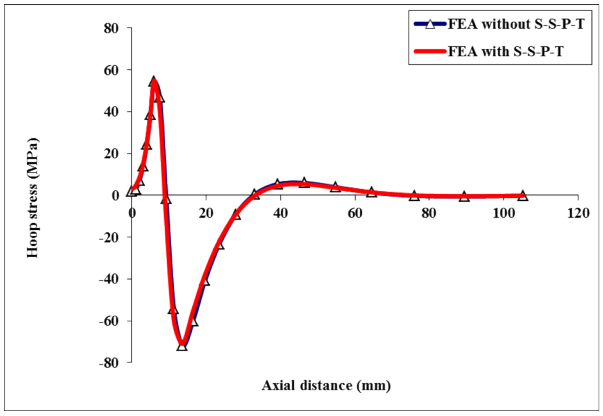

Fig.12
Predicted hoop residual Stresses distribution on the outer surface with and without solid-state phase transformation of S15C pipe**.**

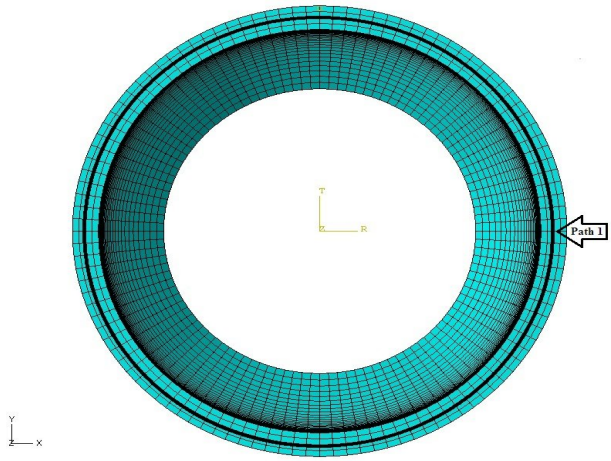

Fig.13
Path 1 for analysis of deformation**.**

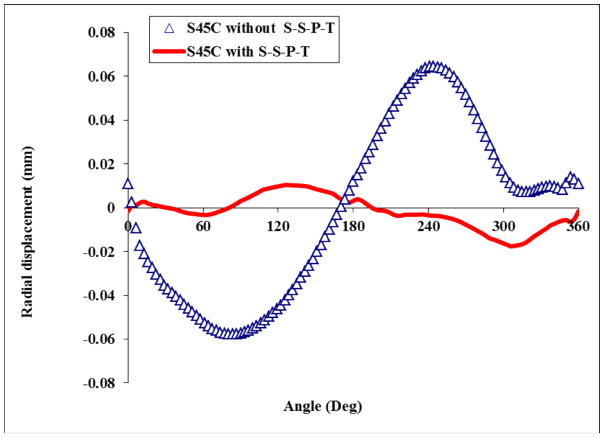

Fig.14
Radial displacement variation in hoop direction at Z=3 mm in HAZ with and without solid-state phase transformation of S45C pipe.

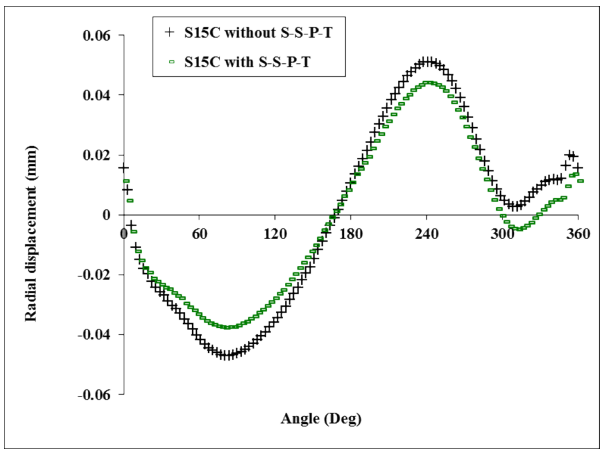

Fig.15
Radial displacement variation in hoop direction at Z=3 mm in HAZ with and without solid-state phase transformation of S15C pipe.

Fig. 14 to 19 show radial, hoop, and axial displacements of S15C and S45C steels with and without considering the effect of phase transformation. It can be observed that for both materials, the values of deformation considering the effect of phase transformation are less than that without it. Also for S45C pipe considering phase transformation effects the sign of radial and hoop displacements have changed.

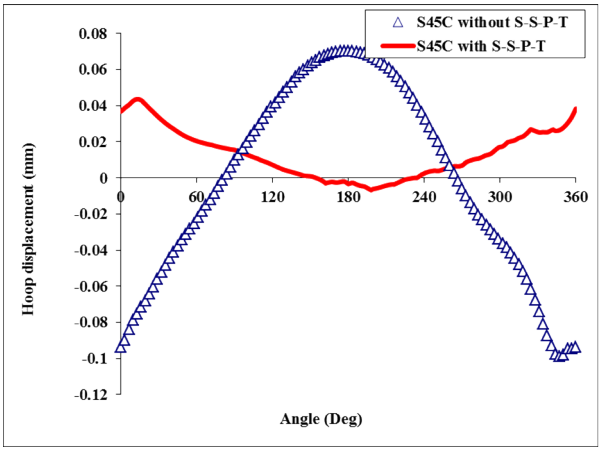

Fig.16
Hoop displacement variation in hoop direction at Z=3 mm in HAZ with and without solid-state phase transformation of S45C pipe.

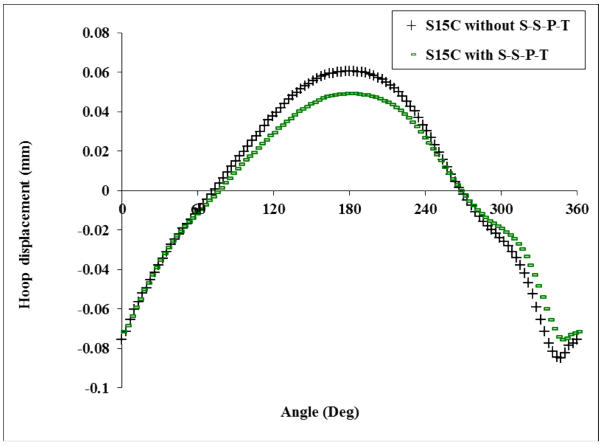

Fig.17
Hoop displacement variation in hoop direction at Z=3 mm in HAZ with and without solid-state phase transformation of S15C pipe.

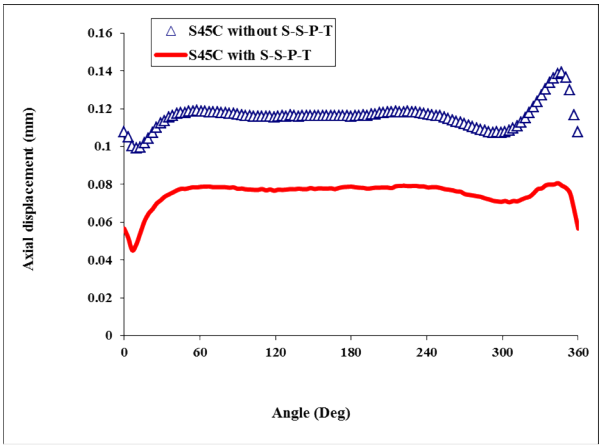

Fig.18
Axial displacement variation in hoop direction at Z=3 mm in HAZ with and without solid-state phase transformation of S45C pipe.

3.2.2. Investigation effect of carbon percentage on welding distortion

Fig. 20 to 22 show the effect of carbon percentage on the radial, hoop, and axial displacements. From these figures, it can be concluded that:

- Without considering the effect of phase transformation the value of displacement of the S45C pipe is more than S15C pipe.
- The temperature range of phase transformation of S45C is lower than S15C pipe, therefore, considering the effect of phase transformation the value of displacement of S45C is smaller than S15C pipe.

3.2.3. Deformations on a cross-section area parallel to the axis of the pipe

In this section, a linear path (path 2 in Fig 23) at θ=140° is defined in the middle of the thickness of a cross-section area parallel to the axis of the pipe, and total deformation and Z- directional displacement of nodes on this path are investigated.

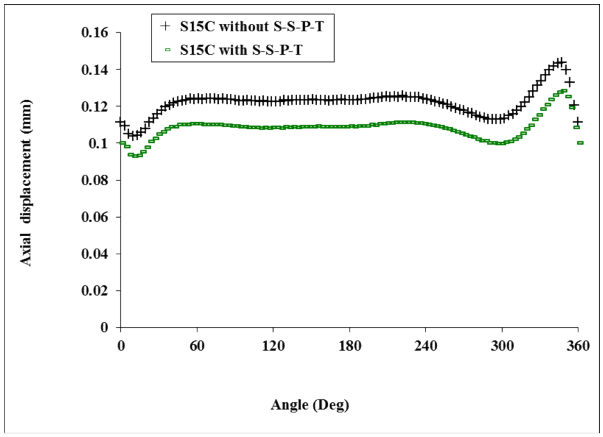

Fig.19
Axial displacement variation in hoop direction at Z=3 mm in HAZ with and without solid-state phase transformation of S15C pipe**.**

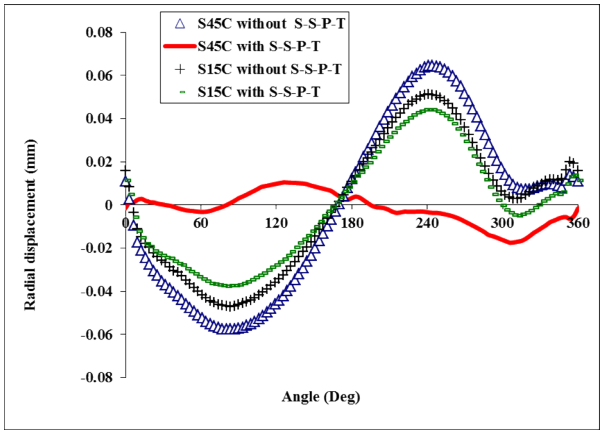

Fig.20
Radial displacement variation in hoop direction at Z=3 mm in HAZ with and without solid-state phase transformation of S15C & S45C pipes**.**

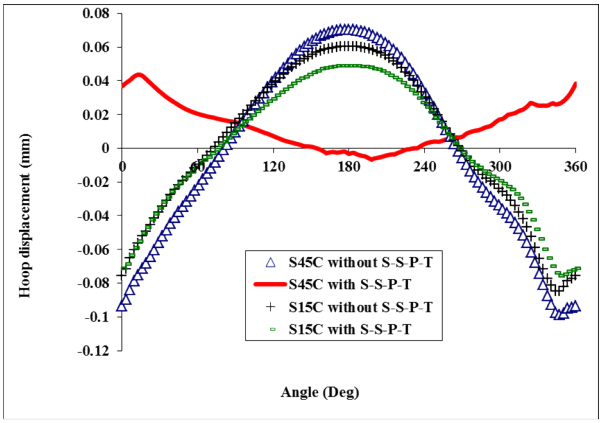

Fig.21
Hoop displacement variation in hoop direction at Z=3 mm in HAZ with and without solid-state phase transformation of S15C & S45C pipes.

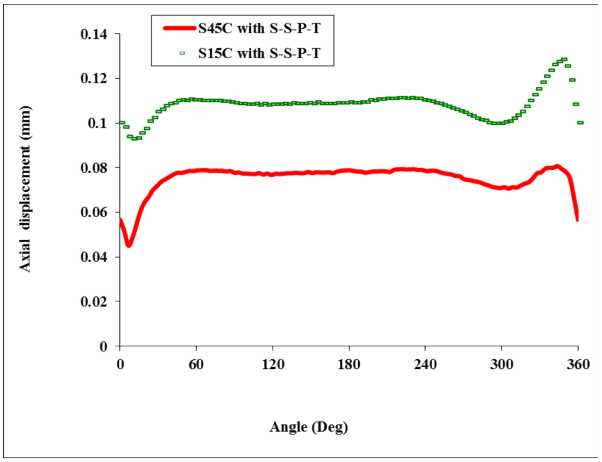

Fig.22
Axial displacement variation in hoop direction at Z=3 mm in HAZ with solid-state phase transformation of S15C & S45C pipes.

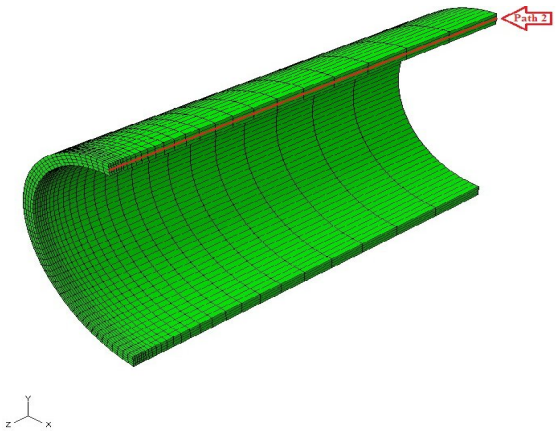

Fig.23
Path 2 for analysis of deformation.

Fig. 24 to 27 show deflections along path 2 with and without considering the effect of phase transformation of S15C & S45C steels. It can be concluded that for both materials the value of total displacement considering the effect of phase transformation is less than that of without it. It can be explained by the volumetric increase of the material that undergoes the austenite to martensite phase transformation.

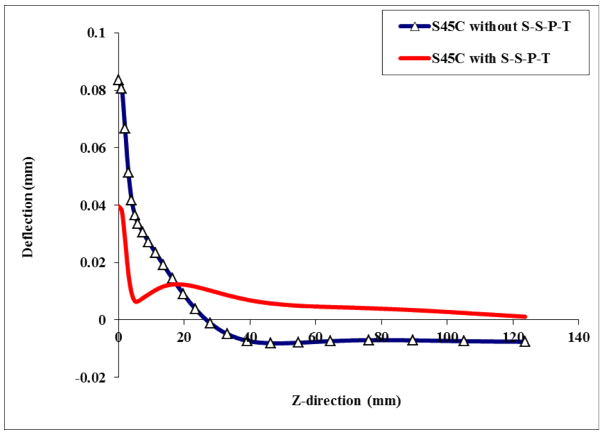

Fig.24
Deflection along path 2 with and without solid-state phase transformation of S45C pipe.

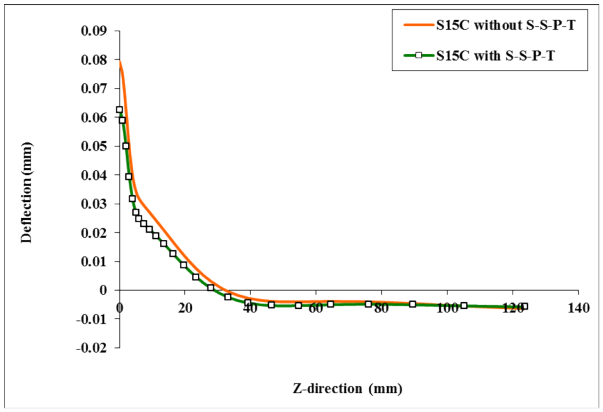

Fig.25
Deflection along path 2 with and without solid-state phase transformation of S15C pipe.

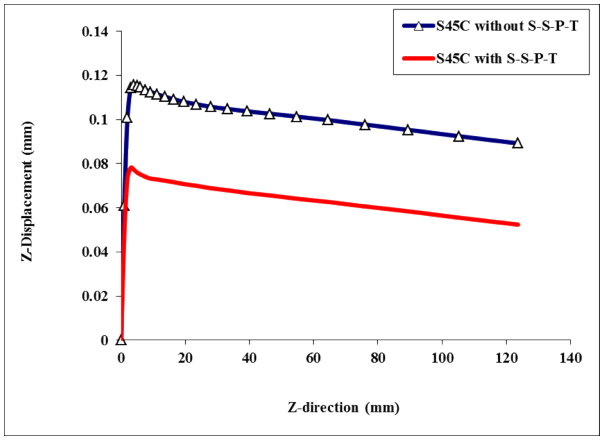

Fig.26
Z-directional displacement along path 2 with and without solid-state phase transformation of S45C pipe.

Fig. 28 and 29 show the effect of carbon percentage on welding deformation. The results indicate that considering phase transformation the total deformation for S45C is smaller than S15C steel. The reason for this exists a large volume dilation in S45C steel relative to S15C steel. Also from figures 28 and 29, it can be concluded that considering phase transformation, the value of deflection and axial displacement for S45C relative to S15C has reduced by 37% and 30%, respectively.

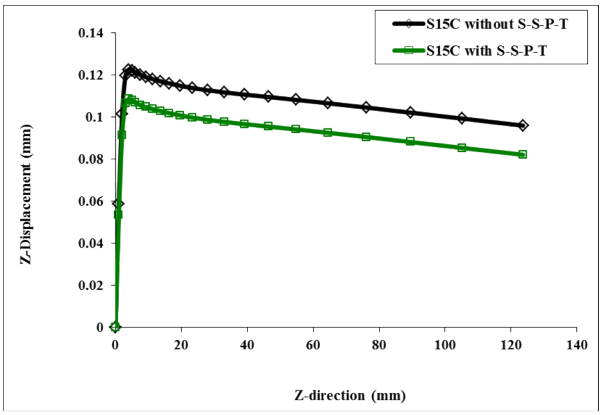

Fig.27
Z-directional displacement along path 2 with and without solid-state phase transformation of S15C pipe**.**

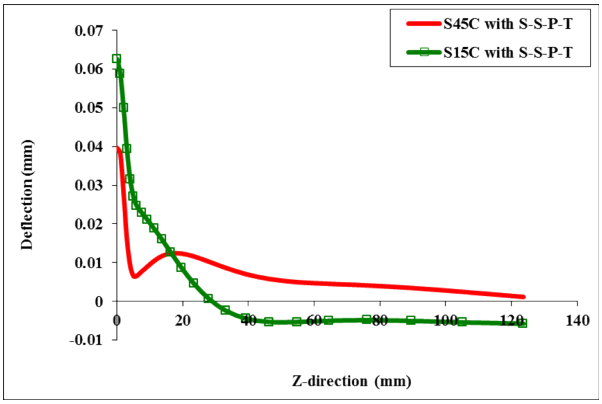

Fig.28
Deflection along path 2 with solid-state phase transformation of S15C & S45C pipes**.**

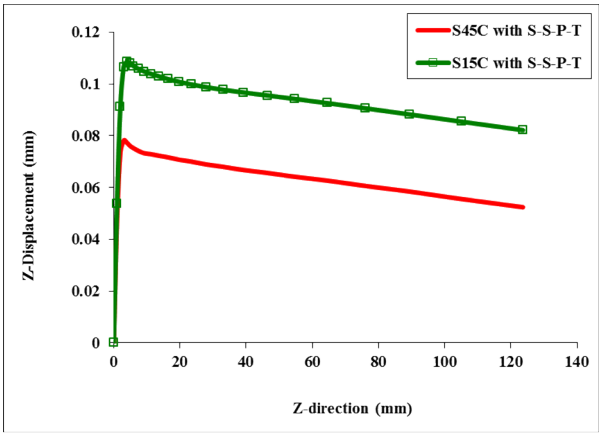

Fig.29
Z-directional displacement along path 2 with solid-state phase transformation of S15C & S45C pipes.

4 CONCLUDING REMARKS

This study developed a sequentially coupled 3-D thermal-metallurgical-mechanical analysis to predict welding residual stresses and distortion during single-pass tungsten inert gas arc welding (TIG) of carbon steel pipes (S45C & S15C) using ABAQUS finite element techniques.

Based on the FE model, the influence of solid-state phase transformation on the axial and hoop residual stresses and distortion was investigated by allowing volumetric change due to solid-state phase transformation.

The simulation results showed that for the S15C pipe, solid-state phase transformation has a very small effect on welding residual stresses and distortion, But for the S45C pipe, it has a significant effect because solid-state phase transformation not only reduces the magnitude of axial and hoop residual stresses and distortion in FZ and HAZ but also alters the sign of hoop residual stresses in FZ.

REFERENCES

[1] Deng.D, Murakawa.Hidekazu, "Prediction of welding residual stress in multi-pass butt-welded modified 9Cr–1Mo steel pipe considering phase transformation effects", Computational Materials Science, 2006; 37:209-219.

[2] A. Yaghi, TH. Hyde, AA. Becker, W. Sun." Finite element simulation of welding and residual stresses in a P91 steel pipe incorporating solid-state phase transformation and post-weld heat treatment", J Strain Anal, 2008; 43:275–93.

[3] Dean Deng, Hidekazu Murakawa," Finite Element Analysis of Temperature Field, Microstructure and Residual Stress in multi-pass butt-welded 2.25Cr-1Mo steel Pipes", Journal of Computational Materials Science, 2008;43:681-695.

[4] Dean Deng," FEM prediction of welding residual stress and distortion in carbon steel considering phase transformation effects", Journal of Materials and Design, 2009; 30:359-365.

[5] Chin-Hyung Lee, Kyong-Ho Chang." Prediction of residual stresses in high strength carbon steel pipe weld considering solid-state phase transformation effects", Computers & Structures, 2011; 89:256-265.

[6] S. Feli; M.E. Aalami Aaleagha; M.R. Jahanban, Evaluation Effects of Modeling Parameters on the Temperature Fields and Residual Stresses of Butt-Welded Stainless Steel Pipes, Journal of Stress Analysis, 2017; 1(2): 25-33.

[7] Sendong Ren, Suo Li, Yifeng Wang, Dean Deng, Ninshu Ma , Finite element analysis of residual stress in 2.25Cr-1Mo steel pipe during welding and heat treatment process, Journal of Manufacturing Processes, 2019; 47, 110-118.

[8] Obeid Obeid, Anthony J. Leslie, Abdul Ghani Olabi, Influence of girth welding material on thermal and residual stress fields in welded lined pipes, International Journal of Pressure Vessels and Piping, 2022; 200, 104777.

[9] Parviz Asadi , Samaneh Alimohammadi, Omid Kohantorabi, Ali Fazli, Mostafa Akbari, Effects of material type, preheating and weld pass number on residual stress of welded steel pipes by multi-pass TIG welding (C-Mn, SUS304, SUS316), Thermal Science and Engineering Progress, 2020; 16, 100462

[10] Rajiv Kumar, H. C. Dey, A. K. Pradhan, K. Albert, J. G. Thakre, M. M. Mahapatra C. Pandey, Numerical and experimental investigation on distribution of residual stress and the influence of heat treatment in multi-pass dissimilar welded rotor joint of alloy 617/10Cr steel, International Journal of Pressure Vessels and Piping, 2022; 199, 104715

[11] J. Goldak, A. Chakravarti, M. Bibby, Metallurgical Transactions B, 1984; 299-305

[12] D. Deng, Y. Luo, H. Serizawa, M. Shibahara, H. Murakawa, JWRI, 2003; 32 (2) 325–333.

[13] Zhang w, Elmer JW, DebRoy T. Modeling and real time mapping of phase during GTA welding of 1005 steel. Marter Sci Eng A2002; 333:320-5.

[14] B. Brickstad, B. L. Josefson, "A Parametric Study of Residual Stresses in Multi-pass Butt-welded Stainless Steel Pipes" Int. J. of Pressure Vessels and Piping, 1998; 75(1):11-25.

[15] SH. Cho, JW. Kim," Analysis of residual stress in carbon steel weldment incorporating phase transformation" Sci Technol Weld Join, 2002; 4:212-6.

[16] DP. Koistinen, RE. Marburger, "A general equation prescribing extent of austenite–martensite transformation in pure iron + zarbon alloys and carbonsteels" Acta Metall, 1959; 7:59–60.

[17] METEQ Ver1.2 CD-ROM, The Society of Material Science, Japan; 2002.

[18] D. Deng, H. Murakawa, Numerical simulation of temperature field and residual stress in multi-pass welds in stainless steel pipe and comparison with experimental measurements, Comp. Mater. Sci., 37(3) (2006) 269-277.

[19] Bhadeshia HKDH, "Developments in martensitic and bainitic steels, role of the shape deformation", Mater Sci Eng A, 2004; P.9-34.